Investigations on the ejection of steel and slag droplets from gas-stirred steel melts

Ingo Hahn and Dieter Neuschütz
Lehrstuhl für Theoretische Hüttenkunde
Rheinisch-Westfälische Technische Hochschule Aachen
D-52056 Aachen, Germany

Abstract

Liquid ejections from gas-stirred melts can be classified into smaller film and jet droplets caused by bubbly bursting and larger splashes resulting from gas channels formed at higher exiting gas velocities. In view of the conditions in ladle metallurgy, experimental investigations were carried out at moderate to small gas flow rates in an arc-heated, bottom-stirred 150 kg steel melting furnace and an 80-l-water tank. Droplets were collected at different heights above the melt level, while gas flow rates, viscosities, surface tensions and slag layer thickness were varied. The number of steel droplets collected decreased strongly with height (in the range 30 to 110 mm) and with size (in the range 0.1 to 1.8 mm). Calculations showed that the entrainment of droplets is strongly influenced by the velocity of upwards flowing gases. While at low flow rates typical for secondary metallurgy (0.1 m/s), only droplets < 50 μm will be entrained, BOF-typical flow rates (20 – 50 m/s) will cause particles up to 500 μm to be carried into the dust removal systems. Higher surface tensions resulted in increased droplet ejection, while higher viscosities led to a decreasing quantity of ejected melt. Slag layers led to a decrease in the ejection of steel droplets and to an increase in ejected slag but they did not completely stop steel ejection, because gas bubbles appear to entrain steel drops when they rise through the slag layer. Bubble bursting in a pure slag system caused large but few slags droplets due to the high viscosity of the slag as compared to the steel melt.

Acknowledgement: Financial support granted by the ECSC, contract 7210-CC-124, is gratefully acknowledged.

Introduction

The injection of gases into melts is a basic operation in process metallurgy to improve heat and mass transfer, to accelerate chemical reactions and to support phase separations. If the gases injected are not completely consumed in the melt, they will eventually escape via the melt surface leading to the ejection of droplets or splashes. Some of the larger ones will fall back into the melt contributing to an enhanced mass and heat transfer between gas phase and liquid. Other larger drops will reach the walls and form accretions on the lining. Most of the fine droplets will be carried out with the offgas and collected in the dedusting units.

A detailed knowledge of the relation between gas flow rate, physical properties of the liquid and the amount and size distribution of the ejected droplets is of great importance to minimize the generation of dust and accretions on the one hand and to optimize heat and and mass transfer between gas and melt via droplets on the other. Whenever a slag layer covers the metal melt, rising gas bubbles will be strongly influenced with respect to movement and size by the different density, viscosity and surface tension of the slag, leading to different ejection patterns and dependencies.

This investigation was carried out in view of the conditions in ladle metallurgy. The experimental tests made use of an arc-heated, bottom-stirred 150 kg steel melting furnace and of an 80-l water tank, which served to visualize certain effects connected to droplet ejections.

Mechanisms of droplet formation

Gases ascending in a liquid may reach the surface either as single bubbles, as bubble clusters, or in the form of gas channels. A characteristic sequence is observed when the linear gas velocity at the surface increases, **Fig. 1**. In each case, the interaction of the escaping gas with the liquid causes ejections of liquid [1-5].

The single bubble reaching the melt surface eventually disrupts the bubble film above it causing many very small film droplets to form, **Fig. 2** [1-3]. The bubble cavity then collapses causing a wave movement that results into a central liquid jet directed upwards forming so-called jet droplets, which are larger than the film droplets.

At high exiting gas velocities, a gas jet breakthrough is observed (**Fig. 1**, to the right) which results in the ejection of much larger splashes [5]. The transition from bubbles to gas channels occurs at gas velocities that can be estimated [6] by means of the equation

$$v_{trans} = 0.325 \left(\frac{\sigma \cdot g \cdot \Delta\varsigma}{\varsigma_{li}^2} \right)^{1/4}$$

where σ and ς_{li} are surface tension and density of the liquid, respectively, g the gravitation constant, and $\Delta\varsigma$ the density difference between liquid and gas.

Both for aqueous solutions and for steel melts, the linear exit velocity of the gas that characterizes this transition is $v_{trans} \approx 0.1$ m/s. When this value is surpassed, massive splashes start to appear which lead to amounts of ejected liquid far beyond the amounts ejected by bubble bursting.

The formation of bubble clusters and of very large bubbles are intermediate phenomena between the single bubble and the gas channel, **Fig. 1**.

Bubble bursting has been extensively investigated in aqueous systems [1-7]. Bubbles always form film and jet droplets as long as the bubble diameter does not exceed a critical value, which is 4.2 mm for water [8]. Per bubble, up to 1000 film droplets with individual diameters of 0.1 to 100 µm are formed, while only up to 10 jet droplets are observed, their diameters being around 0.1 times the bubble diameter [4,7]. Although not very numerous, the jet droplets represent the major mass of ejected liquid. Bubbles well beyond the critical size (in water e.g. 6 mm) do not eject any jet droplets any more upon bursting [8].

In pneumatic steelmaking, the generation of dust is to a great extent caused by bubble bursting and by the formation of film and jet droplets in the size range 0.1 to 100 µm [9-12].

Experimental

Tests on the water model were carried out in a cylindrical plexiglass tank of 640 mm diameter and 250 mm height, giving a capacity of approx. 80 litres liquid. The tests were carried out exclusively with an injector installed at the bottom centre of the tank. A rotary pump supplied air from the atmosphere at constant pressure through a metering device to the injector. The stirring rate could be varied between 0 and 500 l_{STP}/h.

Investigations on the influence of viscosity on the configuration of the bubble swarm and the amount of sprayed liquid were carried out with a capillary nozzle. Solutions with viscosities between 1 cP (pure water) and 124 cP (86.3 wt % glycerine) were prepared and the bubble swarm for a gas flow of 200 l_{STP}/h photographed.

The tests with steel and steel/slag melts were carried out in a pilot plasma melting furnace equipped with two plasma torches containing thoria-doped tungsten electrodes [13,14]. The torches were operated in the AC mode with transferred arcs and without a bottom electrode. Arc currents were typically 1350 A, arc lengths about 240 mm, and plasma gas flow rates 9 m³ (STP) Ar/h per torch. Each heat comprised 150 kg of steel and up to 40 kg of slag. The depth of the steel bath was about 150 mm.

The furnace chamber was closed gastight with pneumatic seals allowing the furnace atmosphere to be selected practically at view. Peripheral ducting around the furnace enabled additional gases to be introduced from the side. Most test runs were conducted under a pure argon atmosphere. This is of particular advantage for carrying out tests where there is no slag cover to prevent oxidation. The atmosphere in the furnace chamber was continuously monitored by a quadropole mass spectrometer. Plain steel scrap was used as starting material for steel melts; the average composition of the scrap is given in **Table 1**.

In the present investigation the furnace crucible was lined with rammed Al_2O_3. In the center of the furnace bottom, a porous refractory nozzle of random porosity was installed for bottom stirring. It consisted of burnt chrome magnesite with an open porosity of 23 ± 5 % volume. The maximum gas flow through the bottom refractory nozzle proved to be 400 l_{STP}/h. For these tests argon was the stirring agent.

To collect the spray near the melt, droplet collectors were manufactured from steel. They were lowered through the furnace lid into a definite position above the melt and held there for a constant period of time. On striking the collector surface, sprayed melt constituents weld together with the steel surface and adhere with great stability to the steel collectors. The drop spectrum collected in this range is considered to be representative for the sprayed drops.

The steel collectors consisted of a cylindrical shell closed at one side, with 200 mm length, an external diamter of 60 mm and a thickness of 1 mm. This shell was mounted on a refractory sensor body, as is used in similar form for a non-reusable immersion sensor in the measurement of temperature and in sampling. **Fig. 3** shows schematically the position of the collector from the side. The droplet collectors were placed into position directly above the porous nozzle for periods of 60 s each. These operations were carried out with the plasma torches switched off.

The variation of surface tension of the steel melts was carried out by varying their oxygen contents. Oxygen as a surface-active element has a strong influence on the surface tension of liquid steel. A high oxygen content was reached by melting scrap in contact with air, a low oxygen content by melting in argon and adding 250 g Al to the melt.

Slags were generated by adding the corresponding quantities of oxide components to the furnace. The compositions of the three synthetic slags investigated were selected to yield clearly different slag viscosities (slag no. 2 versus no. 1) and a somewhat higher density at equal viscosity (no. 3 versus no. 1) The chemical analyses of slag samples taken at the end of the respective melting tests are listed in **Table 2** together with their viscosities and densities. The iron contents in slags no. 1 and 2 are probably due to dispersed metallic iron droplets. In slag no. 3 the iron was present as iron oxide. The viscosities were calculated with Urbain's model [15], the densities calculated from partial molar volumes given by [16]. In addition to the oxides listed the final slags contained small amounts of MgO, Na_2O, K_2O, and TiO_2.

The desired oxide mix was added to the furnace after melt down of the steel scrap. The slag layer thickness was roughly proportional to the mass added, namely 15 – 18 mm for 10 kg of slag, 30 – 35 mm for 20 kg, and 60 – 70 for 40 kg.

The typical gas flow rate through the bottom nozzle was 200 l_{STP}/h. The normal distance of the droplet collector face and the slag surface was 40 to 55 mm.

With slags no. 1 and 3 tests were also made without any steel under the slag melt. In those cases 50 kg of slag components were melted, the gas flow being 200 l_{STP}/h again.

The ejection of droplets from liquids in relation to gas bubbles rising in the liquid and bursting at its surface was investigated with steel and slag melts and with water/glycerine with respect to the following variables: Gas flow rate, bubble size, surface tension, viscosity, and slag layer thickness on the steel melt. The ejection was characterized by the quantity of ejected liquid, the size distribution of the droplets and the height above the melt reached by the droplets.

Results

Quantity and size distribution of ejected droplets as a function of height above liquid

The drops found on the steel collector were in the range 0.1 to 1.8 mm. **Fig. 4** shows the influence of the distance between melt surface and collector face on the quantity of size graded steel drops collected. At distances of 30 to 110 mm between bath surface and collector, the measurements proved that the quantity of collected droplets decreased strongly with increasing distance.

In all cases, the number of droplets found was highest in the smallest size class and decreased with rising droplet diameter. Droplets larger than 1.2 mm were not found beyond 30 mm above the melt surface.

The height above the bath surface reached by a sprayed drop is dependent on its kinetic energy at the moment of ejection, on the angle of ejection, as well as on the velocity of the upwards flowing gases. The kinetic energy of the ejected droplets is normally not high enough to carry them all the way out of the furnace into the dust removal system. However, particles can be carried away with the off-gas, if the gas flow-rate is high enough and the particle is sufficiently small. The "carry-over" condition can roughly be estimated by assuming that the forces acting on the particle are in equilibrium with each other, that the particle be spherical and that Stokes's law be applicable:

Then, the frictional force F_f and the buoyancy force F_b should balance the gravitational force F_g, $F_f + F_b = F_g$, where

$$F_f = 6\,\pi\eta r_p\, v_g, \qquad F_g = \frac{4}{3}\pi\, r_p^3\, \varsigma_p \cdot g, \qquad F_b = \frac{4}{3}\,\pi\, r_p^3\, \varsigma_g \cdot g$$

and where η is the viscosity of the gas, v_g its linear velocity and ς_g its density, and where r_p and ς_p denote the radius and the density of the particle.

With $\varsigma_p >> \varsigma_g$, we obtain a relationship between particle radius and linear gas velocity,

$$v_g = \frac{2}{9} \cdot \frac{\varsigma_p \cdot g}{\eta} \cdot r_p^2$$

Taking, as an example, steel droplets (ς_p = 7 g/cm^3) and BOF off-gas at 1600 °C ($\eta = 6 \cdot 10^{-5}$ kg/ms), the size of particles that can just be transported by the off-gas was calculated and plotted in **Fig. 5**.

While in secondary metallurgy, gas velocities above the melt are typically at or below 0.1 m/s, these velocities reach 20 to 50 m/s in the BOF converter mouth. Hence, only particles smaller then 50 µm can, if at all, be carried over by the off-gas in secondary metallurgy, but in BOF operation, particles up to 500 µm are easily entrained with the off-gas into the dust removal systems.

Influence of surface tension

The influence of the surface tension of the steel melt was investigated by varying the oxygen content of the steel. The effect of deoxidation on the drop quantity gathered by the collector is shown in **Fig. 6**. A distance of 80 mm was fixed between collector and bath surface and the argon gas throughput was adjusted to 150 l_{STP}/h. Lowering the oxygen content from 1000 ppm to 50 ppm led to a rise in surface tension from 1200 to 1700 mN/m [17]. The quantity of drops collected increased significantly from 10 mg to 45 mg.

With larger surface tension, the rupture of the bubble film releases an increased amount of energy which is then available for the creation of upward flow and for the formation of jet droplets.

Influence of viscosity

The influence of viscosity was examined in the water model with water/glycerine mixtures. The photos in **Fig. 7** show the bubble swarm for a gas flow of 100 l_{STP}/h and viscosities of 124 cP (84.3 wt% glycerine), 24 cP (70 % wt% glycerine) and 1 cP (pure water).

The effect of viscosity on the bubble swarm is evident: In solutions with higher viscosity the rate of ascent of the bubble is retarded so that coalescence to larger bubbles takes place at the nozzle outlet. These bubbles rise without further interaction to the bath surface. The reduction in turbulent flow hinders the formation of smaller bubbles. It was observed that the large bubbles had practically no dwell time at the surface. They penetrated the surface directly to burst without retardation. The consequence was massive splashing, which complicated the measurement of the liquid ejected by bubble bursting. With decreasing viscosity more and more small bubbles were formed leading to a rising quantity of liquid ejected by bubble bursting as could in fact be observed in the water model tests.

Results in the presence of slag layers

With increasing quantities of slag, the volume of steel ejected decreased, while the amount of slag ejected increased, **Fig. 8**. The size distribution between 0.1 and 2 mm remained similar to what was found for steel melts without slag layers.

Slag droplets were not detected when only 10 kg of slag were added. This could be attributed to the fact that for thin slag layers the area above the porous plug was kept free of slag by the upward flow pattern of liquid. For larger slag quantities, there was a continuous slag layer on the steel melt leading to joint ejection of steel and slag droplets. As **Fig. 8** shows, there was considerable scatter in the results concerning the volume of collected droplets of steel as well as of slags. Nevertheless, the trend was clearly observed that a thicker slag layer caused less steel droplets and more slag droplets to be ejected. Slag layers on the steel melt could never completely keep steel droplets from being ejected upon bubble bursting.

In **Fig. 9**, the number of droplets collected is shown on the one hand for the case of 40 kg of slag on the steel melt and on the other hand for the case of a pure slag melt. While in the presence of steel melt, the droplets formed were more numerous and smaller, the absence of steel led to the formation of only very few but large droplets. The high viscosity of slags

determines the behaviour of bubble ascent and bubble bursting, as observed similarly in high viscosity water-glycerine mixtures, **Fig. 7**.

In two-phase systems composed of a steel melt and a thick slag layer the low viscosity of steel still has a strong influence on the ejection behaviour, which is only gradually modified by the slag as seen in **Fig. 9**: Slag no. 2 with its higher viscosity caused a shift towards higher droplet sizes and decreasing droplet numbers as compared to slag no. 1.

The fact that even a relatively thick slag layer cannot keep steel droplets from being ejected is in agreement with a model based on the interfacial energies between slags, metals and gases as discussed by Minto [18] and El Gammal [19]. If σ_M and σ_S are the surface tensions of metal and slag melts, respectively, and γ is the interfacial tension between metal and slag phase, a wetting coefficient can defined according to [19] as:

$$p = \frac{\sigma_M - \sigma_S}{\gamma}$$

Depending on the values of p resulting for a given metal-slag-gas system, three ranges can be distinguished, see **Fig. 10**:

Dispersion	for	$p > 1$
Flotation	for	$-1 < p < 1$
Film stability	for	$p < -1$

In the first range, a gas bubble would penetrate the slag layer without entraining any steel so that upon bursting it should only eject slag droplets. In the second range, the bubble has some steel droplets adhering to it so that bubble bursting should result in a mixture of steel and slag ejection. In the third range the bubble is enclosed in a steel film which should lead to more or less pure steel droplet ejection.

The following values for the surface and interfacial tensions have been taken from the Slag Atlas [16] for σ_S and from ISIJ Tables [20] for σ_M and for γ: $\sigma_S \approx 500$, $\sigma_M \approx 1600$, and $\gamma \approx 1300$ mN/m. Hence, $p = 0.85$, which means that the ejection of steel droplets from steel melts covered with relatively thick slag layers can be interpreted as a flotation effect, where the bubbles entrain some steel droplets through the slag layer to the slag surface.

Conclusions

Gases injected into steel melts cause ejections upon leaving the melt which range from very small film droplets via slightly larger jet droplets to massive splashes. Major influencing factors are the linear velocity of the exiting gas (resulting in single bubbles at low and in gas channels at very high speed), the size range of the bubbles, the viscosity and the surface tension of the liquid. Gas bubbles with diameters above a critical value stop causing jet droplets upon bursting.

Slag layers lead to a decrease in the ejection of steel droplets and to an increase in ejected slag but they do not completely stop steel ejection, because gas bubbles appear to entrain steel drops when they rise through the slag layer. This phenomenon can be explained on the basis

of surface and interfacial tensions. Bubble bursting in pure slag systems leads to large but few slags droplets due to the high viscosity of slags as compared to steel melts.

References

1. Gleim, V.T.:
J. Appl. Chem. USSR 26 (1953), pp. 1099/1106

2. Newitt, D.M.; Dombrowski, N.; Knelman, F.H.:
Liquid entrainment - 1. The mechanism of drop formation from gas or vapour bubbles; Trans. Instn. Chem. Engrs. 32 (1954), pp. 244/61

3. Garner, F.H.; Ellis, S.R.M.; Lacey, J.A.:
The size distribution and entrainment of droplets; Trans. Instn. Chem. Engrs. 32 (1954), pp. 222/35

4. Paterson, M.PP.; Spillane, K.T.:
Surface films and the production of sea-salt aerosol; Quart. J. R. Met. Soc. 95 (1969), pp. 526/34

5. I. Kataoka, M. Ishii:
Mechanistic Modeling of Pool Entrainment Phenomenon; Intern. Journal of Heat and Mass Transfer 27 (1984), pp. 1999-2014

6. Voßnacke, A.; Koch, M.K.; Brockmeier, U.; Unger, H.:
Tropfenfreisetzung und Aerosolbildung beim Gasaufstieg durch Flüssigkeitsvorlagen; Ruhr-Universität Bochum, RUB E-97, März 1995, p.19

7. Resch, F.J.; Darrozes, J.S.; Afeti, G.M.:
Marine liquid aerosol production from bursting of air bubbles; J. Geophys. Res. 91 (1986) no. C1, pp. 1019/29

8. Morton, D.; Han, Z.; Holappa, L.:
An investigation of splash formation due to bubble bursting in secondary steelmaking processes; First international conference on process development in iron and steelmaking 7-8 June 1999, Luleå, Sweden.

9. Ohno, T.; Ono, H.; Okajima, M.:
Trans. ISIJ 26 (1986), p. B312

10. Tsujino, R.; Hirai, M.; Ohno, T.; Ishiwata, N.; Inoshita, T.:
ISIJ Int. 29 (1989) No. 4, pp. 291/99

11. Delhaes, C.; Hauck, A.; Neuschütz, D.:
Mechanisms of dust generation in a stainless steelmaking converter; steel research 64 (1993) no. 1, pp. 22-27

12. Nedar, L.:
Dust formation in a BOF converter; steel res. 67 (1996), pp. 320-327

13. Hauck, A.; Neuschütz, D.:
Plasma research facility for melting and heating of metallic and nonmetallic materials; 10th Int. Symp. on Plasma Chemistry, ISPC-10, Bochum, proc. vol. 2, paper 1.5-19, 1991

14. Neuschütz, D.; Zhai, Y.; Hauck, A.:
Nitrogen transfer into plasma heated steel melts as a function of arc polarity; steel res. 65 (1994), pp. 219-224

15. Urbain, G.:
Viscosity estimation of slags; steel research 58 (1987) no. 3, pp. 111/16

16. Slag Atlas, 2nd Edition:
Ed.: Verein Deutscher Eisenhüttenleute, Verlag Stahleisen, Düsseldorf

17. Handbook of Physico-Chemical Properties at High Temperatures; editors Y. Kawai, Y. Shiraishi; The Iron and Steel Institute of Japan, Special Issu. No. 41, 1988, p. 153

18. Minto, R.; Davenport, W.G.:
Entrapment and flotation of matte in slags; Trans. Inst. of Mining and Metallurgy (1972), pp. C36/42

19. El Gammal, T.; Wosch, E.A.T.; Schrinner, H.-J.:
The relationship between surface/interface phenomena and the emulsifying behaviour in the system steel alloy / slag at 1550°C; proc. 5th int. Symp. on molten salt chem. & techn.; Dresden, Germany, Aug. 1997; ed. H. Wendt, pp. 567/74

20. Handbook of Physico-Chemical Properties at High Temperatures; editors Y. Kawai, Y. Shiraishi; The Iron and Steel Institute of Japan, Special Issu. No. 41, 1988, pp. 153 and 170

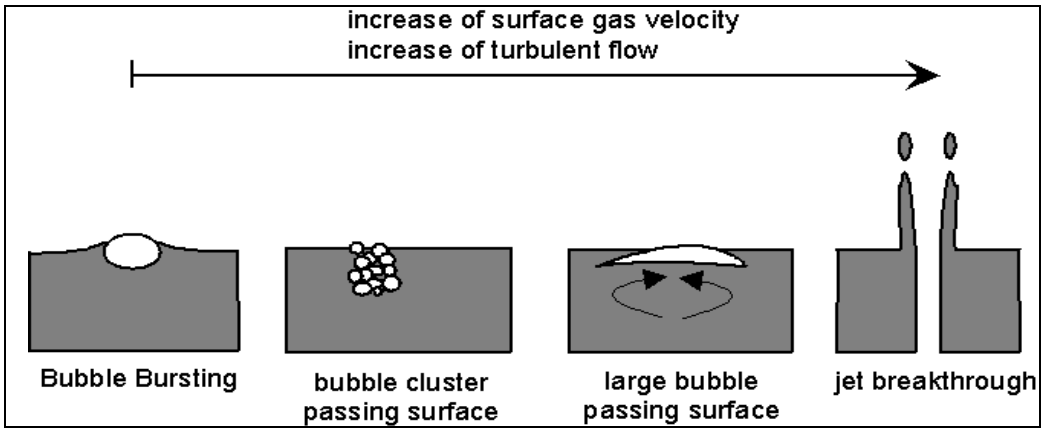

Fig. 1: Different types of interaction of a gas with a liquid surface as a function of gas velocity

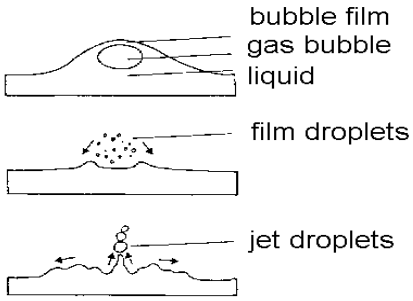

Fig. 2: Mechanism of bubble bursting to form film and jet droplets (after Gleim [1])

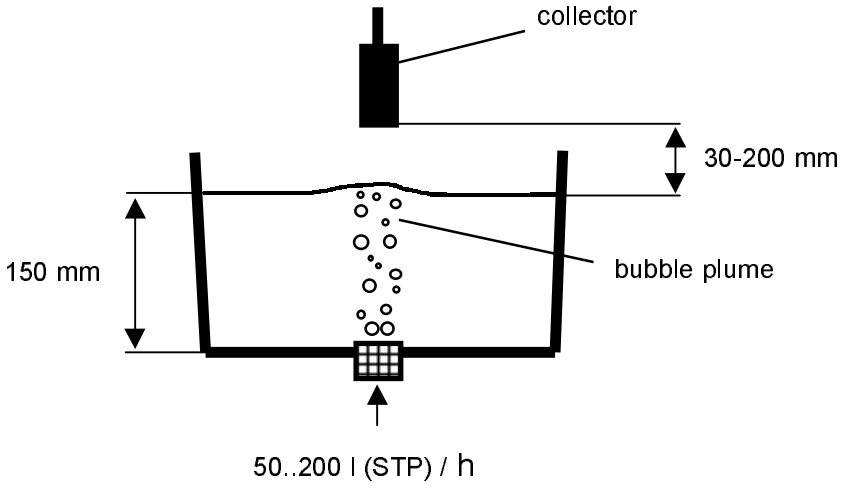

Fig. 3: Side view of crucible during bottom stirring of liquid steel with droplet collector in position above steel melt

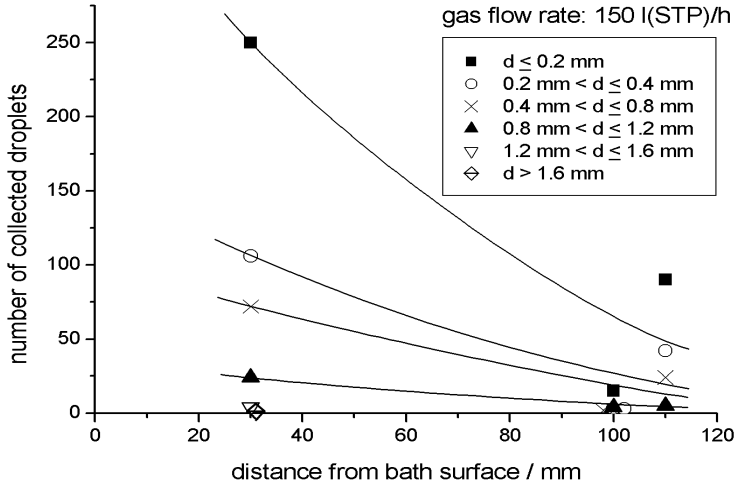

Fig. 4: Influence of distance between melt surface and collector on droplet ejection in size gradings

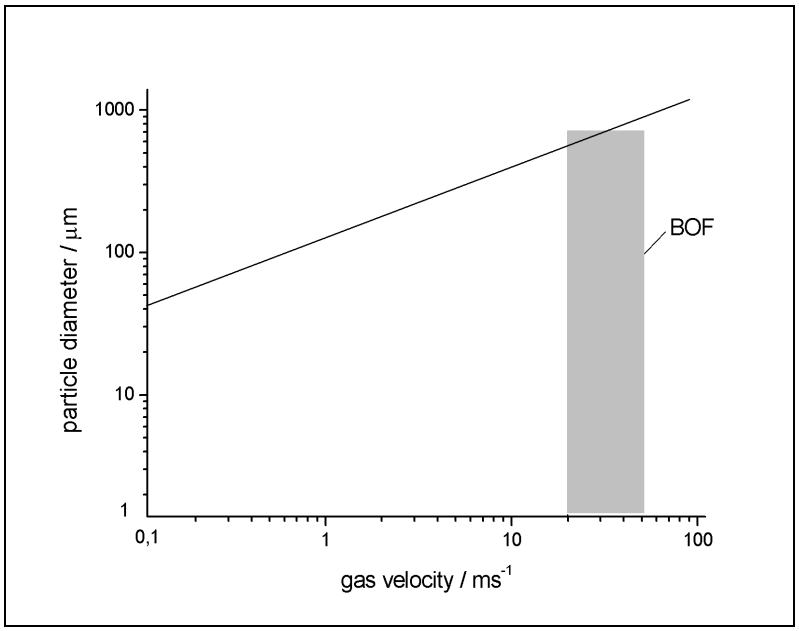

Fig. 5: Balance of forces acting on a particle floating in a gas stream flowing upward.
Partical density: 7 g /cm^3; gas viscosity: $6 \cdot 10^{-5}$ Pa · s

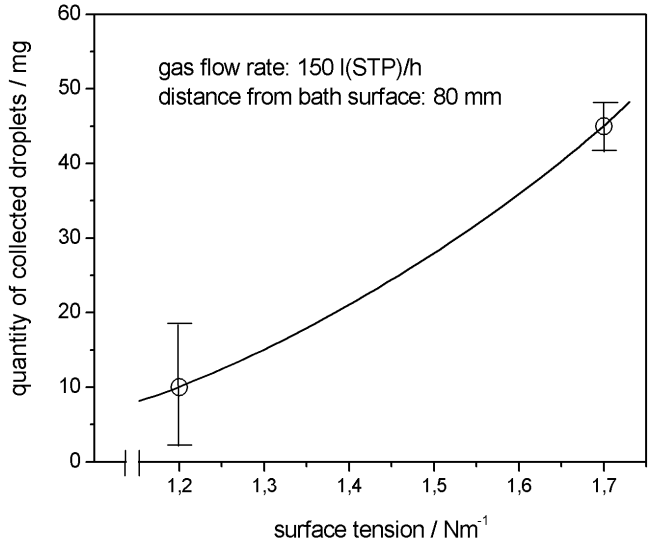

Fig. 6: Influence of the surface tension of liquid steel on the quantity of ejected droplets collected at 80 mm above melt surface

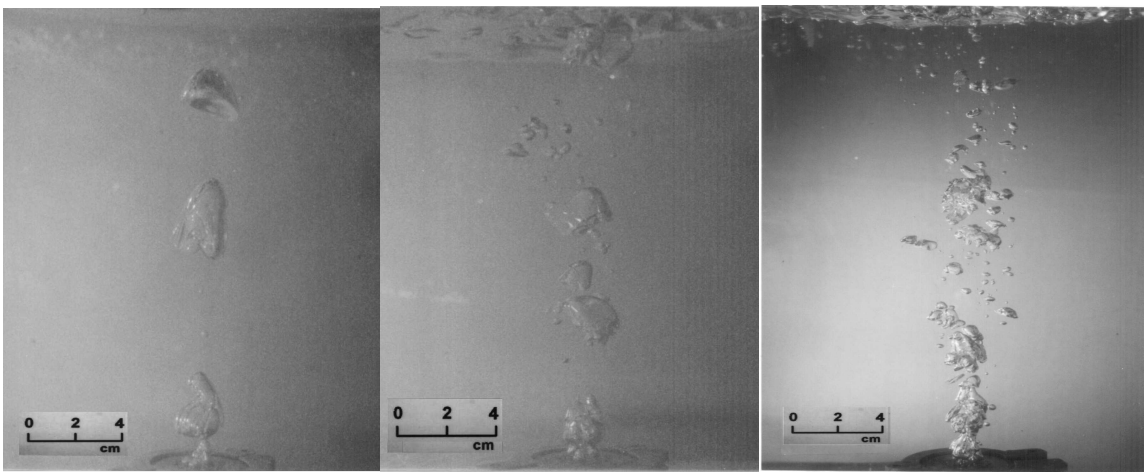

124 cP 24 cP 1 cP

Fig. 7: Influence of the viscosity of water-glycerine mixtures on the shape and number of bubbles at constant gas flow of 200 l_{STP}/h.

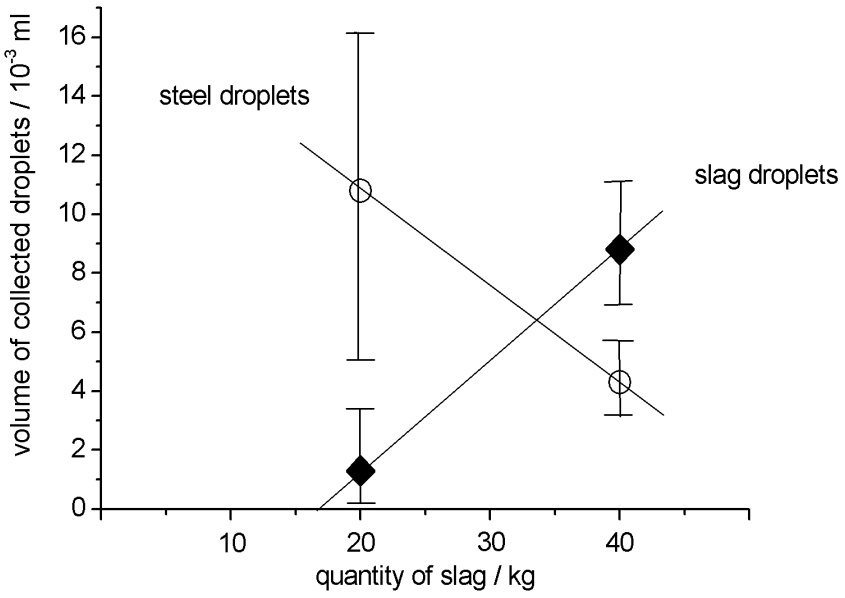

Fig. 8: Influence of the quantity of slag covering the steel melt on the ejection of steel and slag droplets

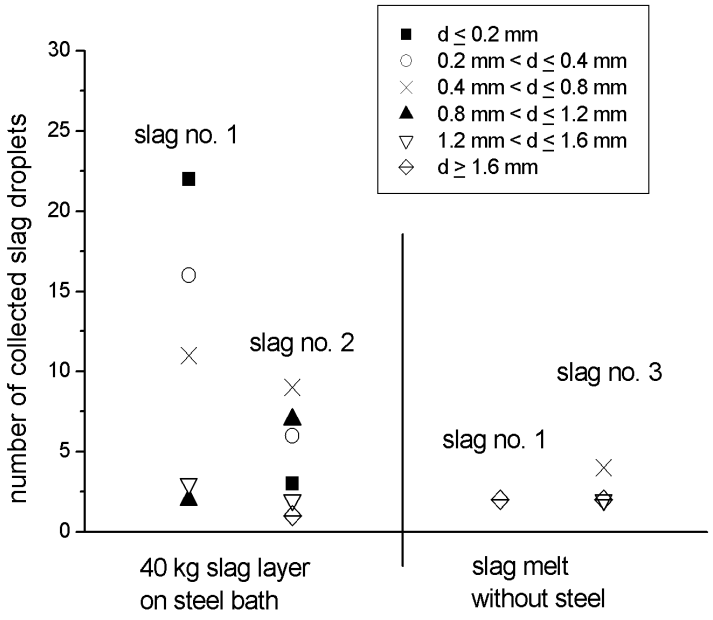

Fig. 9: Comparison of droplet ejection (a) from a steel melt covered with 40 kg of slag and (b) from a pure slag melt. For slag compositions, see **Table 2**.

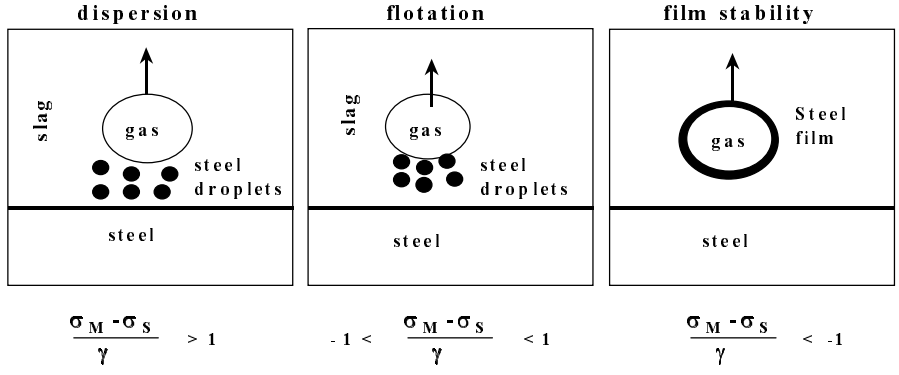

Fig. 10: Three ranges for the behaviour of a gas bubble passing through liquid steel and slag as based on the respective surface and interfacial tensions

Table 1: Composition of the steel scrap in tests (mass contents in %)

C	Si	Mn	P	S	Cr	Ni	Cu	Al
0.069	0.235	1.140	0.019	0.01	0.045	0.037	0.050	0

Table 2: Chemical compositions of synthetic slags and estimated viscosity and density values

Slag no.	Al_2O_3	SiO_2	CaO	MnO	Fe	Viscosity	Density
	mass content in %					η/cP	ς/gcm^{-3}
1	45.5	5.3	47.3	0.4	0.3	440	2.65
2	29.5	34.2	32.6	1.7	0.6	1480	2.81
3	48.7	6.7	30.8	5.3	7.3	590	2.96